Laser-induced crystallization and phase transitions of As_2Se_3 under high pressure

Tomasz Jaroń,[1,*] Vitali B. Prakapenka,[2] and Viktor V. Struzhkin[3,†]
[1]*Centre of New Technologies, University of Warsaw, Banacha 2c, 02-097 Warsaw, Poland and Geophysical Laboratory, Carnegie Institution of Washington, 5251 Broad Branch Road NW, Washington, DC 20015, USA*
[2]*Center for the Advanced Radiation Sources, The University of Chicago, Chicago, Illinois 60637, USA*
[3]*Center for High Pressure Science and Technology Advanced Research, Shanghai 201203, China*

(Received 2 June 2020; revised 2 December 2020; accepted 7 December 2020; published 8 January 2021)

Utilizing the synchrotron x-ray powder diffraction As_2Se_3 has been investigated under high pressure in a diamond anvil cell with hydrogen and neon applied as the pressure media. For both systems the amorphous samples were compressed to ca. 2–3 GPa and heated *in situ* by a laser, which led to their crystallization in the *R*-3 *m*, Bi_2Te_3-type phase. During further compression this phase transforms to the *C*2/*m*, β-Sb_2Te_3-type structure, and they coexist within the pressure range of 21.5–33.0 GPa. The latter phase is observed up to the highest achieved pressure of 52.0 GPa, revealing no signs of reaction with the hydrogen pressure-transmitting medium. The pressure evolution of the volume of the reported phases has been described by the third-order Birch-Murnaghan equation of state. The relative stability of the experimentally detected crystalline phases is confirmed by the density functional theory calculations. The pressure-driven evolution of the As–Se distances and coordination number has been discussed in comparison to the recent findings concerning the amorphous *a*-As_2Se_3 phase.

DOI: 10.1103/PhysRevB.103.014103

I. INTRODUCTION

Arsenic selenide, As_2Se_3, belongs to the family of semiconductors composed of the heavier chalcogenides and pnictogens, which are interesting as materials for infrared optics and thermoelectrics [1,2]. The compounds from this group are covalently bonded network solids, and reveal large structural diversity, ranging from the amorphous glasses to various crystalline polymorphs. The ambient forms—amorphous *a*-As_2Se_3 and crystalline $P2_1/n$, denoted here as I, Fig. 1—show similar features, namely, the short- and intermediate-range order of the former closely resembles that found in the crystal, as manifested by the threefold coordination of As and twofold coordination of Se, and by the premises for the layered structure of *a*-As_2Se_3 [3,4].

At ambient conditions, As_2Se_3, besides the amorphous forms [4,5] and the As_2S_3-type structure ($P21/n$) [6–8], denoted here as **I**, is known to adopt also a metastable As_2Te_3-type structure ($C2/m$) [9,10], **II**, Fig. 1, which is obtained after pressure and temperature treatment (3–5 GPa, 300 °C–650 °C). Both these polymorphs are composed of the layers formed by the folded polymeric chains. However, in the structure **I** the As atoms are surrounded by the three Se atoms in the vertices of a trigonal pyramid, while in structure **II** one As atom is octahedrally coordinated by the six Se atoms, and the second As atom occupies the vertex of the trigonal pyramid formed by the three Se atoms. According to our knowledge, no complete crystal data have been reported for the As_2Se_3 under high pressure. However, as the chemical compounds usually behave in a way similar to their heavier analogs while at lower pressures [11], we have considered in this study also the crystal structures adopted by the heavier siblings of As_2Se_3. As should be expected, they show an increase of coordination number with the rising detection (stabilization) pressure. The structure **III** of Bi_2Te_3 type (*R*-3 *m*) is composed of infinite layers containing octahedrally coordinated As atoms, while in the structures **IV** and **V** the coordination of the As atoms rises to sevenfold and eightfold, respectively.

Recently, a reversible pressure-driven amorphous-to-crystalline transition of As_2Se_3 was reported on a basis of diffraction and Raman experiments, combined with *ab initio* molecular dynamics simulations [4]. These results indicate that, upon compression above ca. 13.5 GPa, the amorphous phase gradually loses its intermediate-range order associated with the layered structure, and turns into a three-dimensional amorphous material. The latter is consistent with the results of optical measurements (absorption and reflectivity), which prove that the gradual closure of the band gap occurs with a clear slope decrease around 8 GPa, related to stiffening of the sample when the interlayer van der Waals forces become comparable to the intralayer forces [5]. During further compression to ca. 40.5 GPa the *a*-As_2Se_3 forms a crystalline phase revealing diffraction signals consistent with a face-centered cubic (fcc) unit cell of $a \approx 9.8$ Å. Unfortunately, the exact structure of the latter fcc phase has not been reported. During decompression the fcc phase remains stable down to ca. 34 GPa, while below this pressure the initial amorphous phase is gradually recreated.

Here we investigate As_2Se_3 under high pressure, firstly crystallizing its glassy form via laser-induced heating under moderate compression up to 3 GPa and measuring the x-ray powder diffraction on further pressurization up to 52 GPa.

*t.jaron@cent.uw.edu.pl
†viktorstruzhkin@yahoo.com

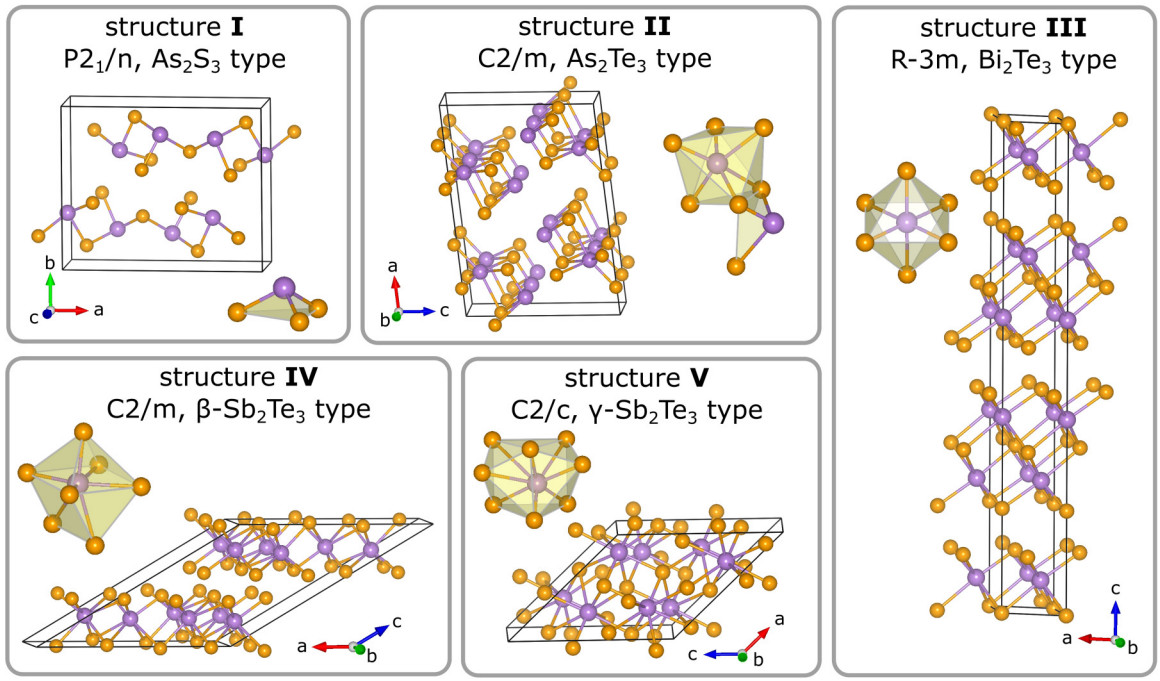

FIG. 1. The crystal unit cells and the coordination environments of As in the most important structures of As_2Se_3 and its heavier siblings considered in this work. As—purple balls; Se—yellow balls.

Bearing in mind the former predictions [12–14] and the recent proofs for hydrogen-related superconductivity [15–18], we have also compared the behavior of the samples in a hydrogen pressure-transmitting medium (PTM) to that in a neutral (neon) medium to check the possibility of high-pressure hydrogenation. The periodic, solid state DFT calculations are used as support in interpretation of the experimental data.

II. EXPERIMENTAL AND COMPUTATIONAL DETAILS

As_2Se_3 glass (99.999%, Alfa Aesar) and Au pressure standard (99.999%, Alfa Aesar) were loaded into the diamond anvil cell (DAC). Diamonds of 200–300 μm culets and rhenium gaskets were used. Ne and H_2, loaded at ca. 170 MPa in the custom-designed gas loading systems at GL, CIW and GSECARS, APS [19] were applied as PTM.

High-pressure angle-dispersive x-ray diffraction (XRD) measurements were performed using the Advanced Photon Source synchrotron facility of Argonne National Laboratory. The measurements were carried out on sectors 13ID-D and 16ID-B operating at wavelengths of 0.3344 Å (beam size 3–4 μm) and 0.3547 Å (beam size 4–5 μm), respectively. The sample to detector distance and other geometrical parameters were calibrated using LaB_6 or CeO_2 standards. The samples were heated by the double-sided laser systems available at the beamlines to the maximum temperature of up to 1600 K measured by fitting graybody thermal radiation [20]. For each sample heating was carried out in several pulses lasting a few seconds, until the appearance of clear signs of the crystalline phase; the overall amount of energy absorbed by the sample was not monitored. The heating was not uniform across the sample, which has manifested especially for H_2 PTM as variable amounts of amorphous and crystalline phases in various areas of the sample.

The two-dimensional diffraction images were analyzed and integrated using the DIOPTAS software [21]. The crystal structures were refined in JANA2006 [22]. The pseudo-Voigt function with Simpson correction for asymmetry was utilized for modeling of the diffraction peak shape. The background was corrected by Legendre polynomials, while for the data of worse quality manual correction was applied. One overall isotropic thermal parameter was refined for each phase. In the case of phase **III** (As_2Se_3 compressed in H_2) the anisotropic strain broadening was modeled using the tensor approach according to Stephens [23]. The quality of diffraction data for phase **III** in the H_2 PTM allowed for Rietveld refinement with no correction for preferred orientation. Phase **IV** revealed worse pattern averaging in both pressure-transmitting media. Rietveld refinement of this phase compressed in Ne required March-Dollase correction in the [1 1 1] direction, related to the most intense diffraction peak. Although phase **IV** compressed in H_2 revealed better powder averaging, and was refined without the correction for preferred orientation, it showed low intensity in comparison with the amorphous As_2Se_3, Fig. S6 (see Supplemental Material [24]). The lattice parameters of the systems not shown in Figs. S5–S7 [24] were obtained on a basis of Le Bail refinement or were estimated from *d* spacings. The structure of phase **III** at 3 GPa has been deposited in the ICSD database, deposition number 2007150. The equations of state (EOS) were fitted using the EOSFIT7-GUI program [25,26].

Theoretical optimization of the crystal structures was performed using density functional theory (DFT), as implemented in the CASTEP program [27] contained in the MATERIALS STUDIO package (Biovia). The generalized gradient approximation (GGA) with the PBE correlation-exchange functional and ultrasoft Vanderbilt-type pseudopotentials were used. Both unit cell vectors and atomic coordinates

were optimized using the Broyden-Fletcher-Goldfarb-Shanno (BFGS) algorithm. A 330-eV cutoff and a k-point grid density of ca. 0.06 $Å^{-1}$ were used for the final optimizations and calculations of total enthalpy. Although in our calculations the static enthalpies were computed for $T = 0$ K, the findings can be still valid at room temperature due to rather insignificant entropic effects and vibrational zero point corrections for the solid systems composed of heavier elements (in fact, these effects are often ignored even for the systems containing light elements) [28,29]. The electronic self-consistent field (SCF) convergence remained 5.0×10^{-7} eV per atom, while the convergence criteria for geometry optimization were set as follows: energy change 5.0×10^{-6} eV per atom, maximum force 0.01 eV $Å^{-1}$, maximum stress 0.02 GPa, and maximum displacement 5.0×10^{-4} Å. The calculations have been carried out for the primitive representations of the unit cells (whenever applicable).

III. RESULTS AND DISCUSSION

Upon moderate compression to ca. 2–3 GPa the samples of As_2Se_3 remain amorphous, regardless of PTM used; see Fig. 2 and Figs. S1 and S2 in the Supplemental Material [24]. The *in situ* laser heating was performed as several pulses lasting a few seconds each, until a crystalline phase appeared. The sample in the H_2 PTM was only partially crystallized, which resulted in rather uniformly distributed crystallites embedded in the remaining a-As_2Se_3. On the other hand, the sample in the neon PTM crystallized completely, and much fewer, large crystallites were formed. Consequently, very spotty diffraction signals were observed for this sample, Figs. S10 and S11 [24], which strongly influenced the relative peak intensities on the integrated diffraction pattern. The same set of reflections is observed in both systems, which corresponds to the Bi_2Te_3-type structure **III**, Fig. 1, as it has been confirmed by Rietveld refinement, Fig. S5 [24]. Besides the signals from phase **III**, also the diffraction peaks from unknown phase(s) are observed in both samples—either as a minor contribution to the pattern (for the As_2Se_3–H_2 system) or as moderate to intense peaks (for the As_2Se_3-Ne system). However, due to the pronounced strong texture present in the latter system, the integrated intensities are less meaningful there. Closer inspection reveals that this phase is represented by much fewer crystallites than phase **III**, Fig. S9 [24].

During further increase of pressure to 21.5 GPa and above a different set of diffraction peaks appears and gradually increases its intensity relative to the signals from phase **III**. The emergent phase coexists with phase **III** up to ca. 33.0 or 30.3 GPa, as observed in the As_2Se_3–H_2 and As_2Se_3-Ne systems, respectively. In the As_2Se_3-Ne system the phase transition leads to significant improvement of the quality of the diffraction patterns, Fig. S11 in the Supplemental Material [24], especially at higher pressures (although still remaining far from perfect averaging). Among the structures of related compounds, structure **IV**, Fig. 1, allows for the most reliable generation of emerging diffraction peaks. Therefore, this structure has been used for Rietveld refinement (with preferred orientation introduced for the sample in Ne), whenever it was justified by the quality of measured patterns, Figs. S6 and S7 [24]. Phase **IV** compressed in H_2 revealed better

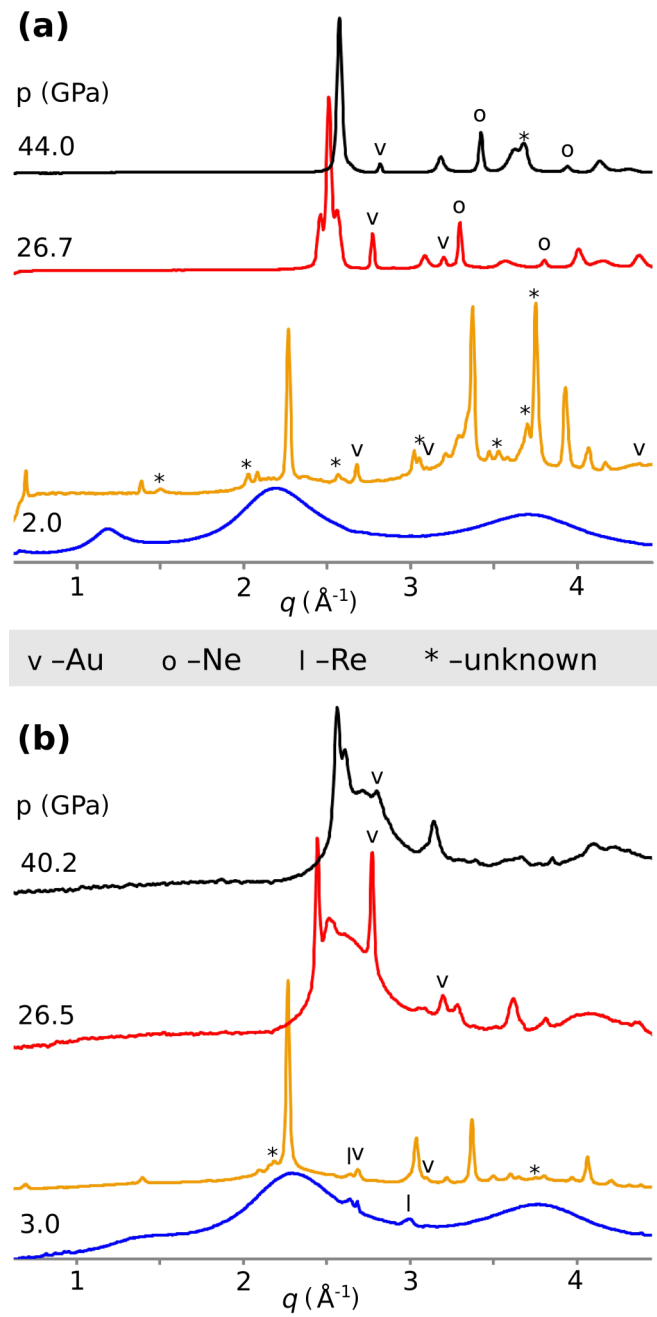

FIG. 2. The x-ray powder diffraction patterns of As_2Se_3 compressed in (a) Ne ($\lambda = 0.3344$ Å); (b) H_2 ($\lambda = 0.3547$ Å). The patterns from amorphous samples, measured before laser heating, are shown at the bottom of each dataset (and also from liquid Ne pressure medium below 4 GPa, if applicable).

powder averaging, which allowed for refinement without a correction for preferred orientation, Fig. S6 [24], although still not all the diffraction peaks were sufficiently well modeled in this approach, in contrast to Le Bail refinement. As mentioned above, the crystalline phase remains surrounded by a significant amount of amorphous matrix in the latter system, which resulted in weaker signals relative to the background, Fig. S6 [24]. While the results obtained for both systems indicate the presence of the same crystalline phases, the phase transition seems facilitated in the system containing Ne as

PTM. Consequently, achieving a similar relative amount of phase **IV** vs phase **III** requires pressure 3–5 GPa lower than for the system utilizing H_2 as PTM. Such behavior could be influenced by slightly worse hydrostaticity of Ne, compared to H_2 PTM [30,31], or by different sample form—fewer, larger crystallites in Ne PTM, and numerous smaller crystallites embedded in the amorphous matrix of a-As_2Se_3 in H_2 PTM. A similar phase transition from structure **III** to structure **IV** has been reported for the heavier analogs of As_2Se_3: for Sb_2Te_3 this $C2/m$ phase forms at ca. 9 GPa [29,32], while $C2/m$ Bi_2Te_3 has been detected around 8 GPa [33,34], i.e., close to the pressure necessary for induction of superconducting properties for this topological insulator [35]. Interestingly, under hydrostatic compression of As_2Te_3 a direct phase transition between structures **II** and **V** is already observed above 17.4 GPa [36–38]. In this case, phase **III** has been observed only under nonhydrostatic conditions due to a large kinetic barrier expected between structures **II** and **III** [36,39,40].

Phase **IV** of As_2Se_3 remains stable up to 52 GPa—the highest pressure reached here in the As_2Se_3–H_2 system. Our data indicate that the pressure medium does not influence the identity of detected phases—the same set of reflections is observed for both samples over the entire pressure range studied, while the coexistence of phases **III** and **IV** is shifted towards slightly higher pressures for the H_2 PTM, Figs. S3 and S4 in the Supplemental Material [24].

Some amount of the amorphous phase (a-As_2Se_3) still can be detected in the sample compressed in hydrogen over the entire pressure range studied. The relative intensity of the broad diffraction signals from the amorphous phase strongly varied for different areas of the sample, which is related to the not uniform laser heating, resulting in nonhomogeneous crystallization. We have not found clear evidence for sample reamorphization, i.e., a monotonic relation between the intensities of crystalline and amorphous phases, Fig. S1 [24]. Surprisingly, the signals from a-As_2Se_3 are observed in the whole pressure range studied, up to 52 GPa, while, as it has been mentioned above, Ahmad *et al.* [4] reported crystallization of a-As_2Se_3 above 40 GPa, forming a crystalline phase with diffraction peaks that can be indexed in an fcc unit cell, with $a \approx 9.8$ Å. However, the structure of this phase has not been solved, and the details of its diffraction patterns and pressure of crystallization were significantly influenced by the pressure medium used. This phase has not been unambiguously detected in our current experiments.

The molecular volumes of the As_2Se_3 crystalline phases measured in both pressure media remain very close in the whole investigated pressure range, Fig. 3. Identical crystalline structures adopted by As_2Se_3 in hydrogen and in neon pressure media, and the lack of volume increase for the As_2Se_3 pressurized in H_2 clearly indicate that hydrogen does not react chemically with As_2Se_3 under the experimental conditions applied. During this first-order phase transition a volume contraction of ca. 5% is observed, which slightly exceeds the 2% or 3% changes reported for the related structures of Sb_2Te_3 and Bi_2Te_3 [29,34]. The obtained pressure–volume data for these phases were fitted to the third-order Birch-Murnaghan equation of state (EoS) [41,42]. For a successful reproduction of the experimental data for the phase **III**, B_0' was initially refined and then fixed at 8, which finally led to

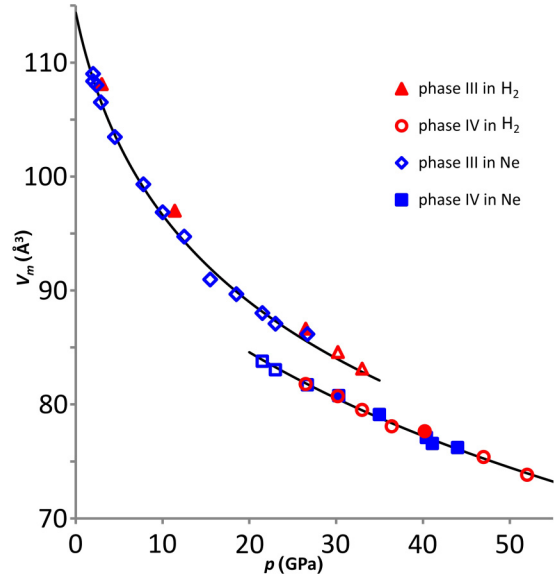

FIG. 3. The molecular volume of phases **III** and **IV** of As_2Se_3 as a function of pressure. The refined values have been presented as the filled symbols; the volumes estimated on the basis of measured d spacings are shown as the open symbols.

$V_0 = 114.4(9)$ Å^3 and $B_0 = 31.2(21)$ GPa. For the phase **IV** the first pressure derivative of the bulk modulus, B_0', was fixed at 4, and the values of the ambient pressure molecular volume, $V_0 = 96.9(9)$ Å^3, and the bulk modulus, $B_0 = 112(8)$ GPa, were obtained.

The bulk modulus of phase **III** is slightly smaller than most of the values reported for its heavier analogs, e.g., α-Sb_2Te_3: $B_0 = 36.1(9)$ GPa for $B_0' = 6.2(4)$ [32] and $B_0 = 54.7(2)$ GPa for B_0' fixed at 4 [29]. A similar trend has been observed for α-A_2Te_3, A = As–Bi, which is related to the increased compressibility of the lightest compound in the interlayer direction. In this case, the larger compressibility of the van der Waals distances overcompensates the stiffer covalent intralayer bonds (cf. the discussion in the Supporting Information of Ref. [36]). Phase **IV** is much less compressible in comparison to its heavier analog, β-Sb_2Te_3. The latter is characterized by the B_0 values of 62(3)–77.1(5) GPa obtained for B_0' fixed at 4 [29,43]. In this quasi-three-dimensional (3D) phase the layers have already been squeezed significantly, approaching the pnictide and chalcogenide atoms closer than the sum of their van der Waals radii (ca. 3.7 Å for As $\cdots$ Se). The latter, originally "interlayer" distances, became very close to the "intralayer" distances, Fig. 5. For such substantially well-packed structures, the bulk moduli of the isostructural and closely related compounds (in terms of bonding character) may be scaled approximately with their molecular volumes (which serve as a measure of average interatomic distance), according to Eq. (1):

$$B_0^A = B_0^B \left(\frac{V_0^B}{V_0^A} \right)^m, \tag{1}$$

where B_0^A, B_0^B, V_0^A, and V_0^B are the bulk moduli and the molecular volumes of the isostructural compounds A and B, while m is a parameter derived from the experimental data ($m =$

TABLE I. Comparison of scaling of bulk modulus for related materials: B_0^A calc.—the bulk modulus of A as obtained from scaling the bulk modulus of B according to Eq. (1); in all the fits the B_0' has been fixed to 4.

	A	B	A	B	
phase	γ-As_2Te_3[a]	γ-Sb_2Te_3[b]	As_2Se_3, **IV**	β-Sb_2Te_3[b]	β-Sb_2Te_3[c]
B_0 (GPa)	95.5(9)	80.5(6)	112(8)[d]	77.1(5)	62(3)
V_0 (Å^3)	117.5(2)	140.0(6)	96.9(9)[d]	148.5(8)	ca. 149
B_0^A calc. (GPa)	–	98.5	–	126	102
Discrep. (%)	–	+3.3	–	+13	–9

[a]Reference [37].
[b]Reference [29].
[c]Reference [43].
[d]This work.

4/3 is obtained immediately from a simple model of ionic compounds [44], while a recent approach for the covalent compounds uses $\underline{m} = 3.46/3$) [45]. This simplistic equation may serve as an initial probe for evaluation of the obtained values of B_0. Considering the dense phases of pnictide chalcogenides, Table I, this approach reveals that bulk moduli, B_0^A calc., estimated on the basis of relative molecular volumes, fall not very far from the values fitted to the experimental data. Elastic properties of amorphous As_2Se_3 were studied at a lower-pressure region via measuring sound velocities.

Compared to the present results for crystalline phases, a-As_2Se_3 is characterized by lower values of bulk modulus: $B_0 = 14.4$ GPa for $B_0' = 8.1$, and $B_0 = 14.6$ GPa for $B_0' = 6.6(4)$, as reported by Soga *et al.* and by Nichols *et al.*, respectively [46,47].

To support the conclusions based on our experimental data we have performed the DFT calculations to elucidate the relative stability of the considered structures at various pressures. This is also relevant for checking the refinement of the atomic positions, which may be significantly biased by the limited quality of the diffraction patterns measured *in situ* under high pressure. The calculated relative enthalpies correspond very well to the sequence of crystalline phases observed for As_2Se_3, Fig. 4(a). According to our calculations, structure **I** is the most stable polymorph at ambient pressure, and is favored by 17 meV per formula unit (f.u.) over structures **II** and **III**; the enthalpies of the latter two phases are virtually equal. However, above ca. 0.5 GPa phase **III** becomes the phase of the lowest enthalpy and remains the most stable phase up to ca. 26 GPa, when phase **IV** should be formed. The latter would remain thermodynamically stable, with respect to phase **V**, up to about 80 GPa, as judged by a linear extrapolation of the calculated data points. The calculated molecular volumes remain very close to the experimental ones, Fig. 4(b), with the relative error of up to +2% for most of the values. Such discrepancy is typical for the DFT calculations using the GGA functionals [48]. The detailed parameters of the experimental and calculated crystal structures has been compared in Table II, and listed in the Supplemental Material [24].

The crystalline phases obtained by *in situ* laser-induced crystallization of a-As_2Se_3 under high pressure differ from those reported earlier for this compound, i.e., phases **I** and **II**. Although Lityagina *et al.* [9] also reported a trigonal form of As_2Se_3, neither its unit cell nor diffraction pattern corresponds to the characteristics of phase **III**. On the other hand, several crystalline phases are very close in terms of enthalpy, which is evident especially in the low-pressure range, Fig. 4(a). In

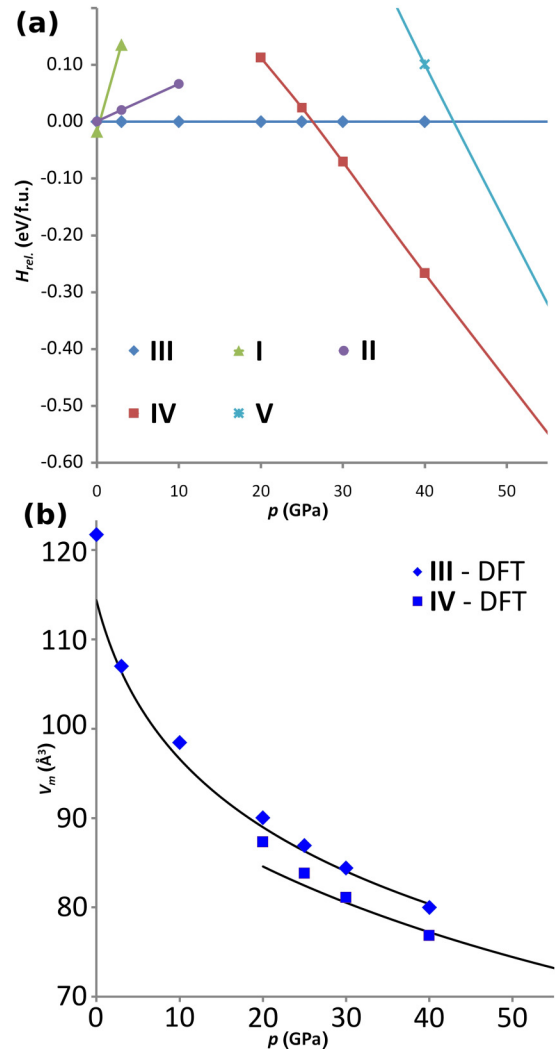

FIG. 4. (a) The calculated enthalpy (per formula unit, f.u.) of several crystalline phases known for As_2Se_3 and related compounds. The values of enthalpy have been normalized to the enthalpy of phase **III**. (b) The comparison of the calculated volume and the equation of state derived from the experimental data.

TABLE II. The refined and calculated parameters of the unit cells of As_2Se_3 at lower- and higher-pressure regions.

Phase	p (GPa)	Lattice parameters (Å)	Atom	x	y	z
III, R-3 m—experimental, As_2Se_3-H_2	3.0	$a = 3.7280(3)$	As1	0	0	0.3987(4)
		$c = 26.946(6)$	Se1	0	0	0
			Se2	0	0	0.2133(2)
III, R-3 m—calculated	3.0	$a = 3.7274$	As1	0	0	0.39785
		$c = 26.678$	Se1	0	0	0
			Se2	0	0	0.2151
IV, $C2/m$—experimental, As_2Se_3-H_2	40.2	$a = 12.05(3)$	As1	0.109(16)	0	0.163(16)
		$b = 3.509(3)$	As2	0.518(14)	0	0.251(14)
		$c = 14.52(4)$	Se1	0.251(8)	0	0.422(8)
		$\beta = 149.61(7)^\circ$	Se2	0.582(13)	–0.5	0.641(13)
			Se3	–0.174(9)	–0.5	–0.023(9)
IV, $C2/m$—calculated	40.0	$a = 12.399$	As1	0.166	0	0.188
		$b = 3.386$	As2	0.445	0	0.219
		$c = 14.703$	Se1	0.223	0	0.393
		$\beta = 150.13^\circ$	Se2	0.559	–0.5	0.629
			Se3	–0.134	–0.5	0.004

these phases, As_2Se_3 adopts several modes of coordination and topologies—As can be coordinated by three to six Se atoms in a few geometries. This may impose the system to be locally frustrated between the crystalline phases and facilitate the formation of the glassy a-As_2Se_3, which occurs reversibly even after pressure-induced crystallization, as noticed by Ahmad *et al.* [4]. The reported crystalline phase of the cubic unit cell formed during pressurization of a-As_2Se_3 to ca. 40 GPa has not been fully identified. However, its volume corresponds very well to the volume of 12 As_2Se_3 f.u. of phase **IV** under this pressure. Among the A_2X_3-type compounds with 12 f.u. present in a cubic unit cell only the Bi_2O_3 structure in the $I23$ space group has been found in the ICSD (retrieved 29.11.2019) [49]. However, this phase is strongly unfavorable energetically in the whole pressure range studied, Fig. S12 [24], and is characterized by a different diffraction pattern than that reported by Ahmad *et al.* [4].

Interestingly, the results of As and Se K-edge extended x-ray absorption fine structure (EXAFS) analysis of a-As_2Se_3 by Properzi *et al.* [50] suggest that no increase in coordination number (N) is observed and N(As–Se) = 3, N(Se–As) = 2 up to 30 GPa. At the same time, the mean first-neighbor As–Se distance increases during compression from ca. 2.42 Å close to 0 GPa (similar values were obtained previously using EXAFS and energy-dispersive x-ray diffraction) [51,52] up to ca. 2.44 Å at 30 GPa. These results suggest that the average densification of the amorphous materials is achieved by compression of the second and further coordination spheres. A similar phenomenon has been observed in a-As_2S_3, where the average As–S distances increase by 0.06 Å within the range of 15–50 GPa [53]. However, in the latter case the elongation of the nearest-neighbors distance is interpreted as a signature of increase of the local coordination number, and a gradual transition from the pyramidal units towards the polyhedral containing more ligands. Such behavior has been observed in a-As_2O_3, increasing the average coordination number of As from 3 to almost 5 between 17 and 32 GPa [54]. The minimal, average, and minimal interlayer As–Se distances in the most stable crystalline phases of As_2Se_3 considered by us have been plotted in Fig. 5. Our theoretical and experimental results indicate that the transitions from phase **I** (theoretically the most stable at 0 GPa) to phase **III** (the most stable within 3–25 GPa), and from phase **III** to phase **IV** (the most stable from 30 GPa) are indeed related to a 5%–10% increase in the average d(As–Se). Such abrupt changes are the effect of switching in coordination number, N(As–Se), from 3 (**I**), through 6 (**III**) up to 7 and 8 (**IV**). Similar evolution should occur in the amorphous phase. However, as the average coordination number plays a role in this case, it

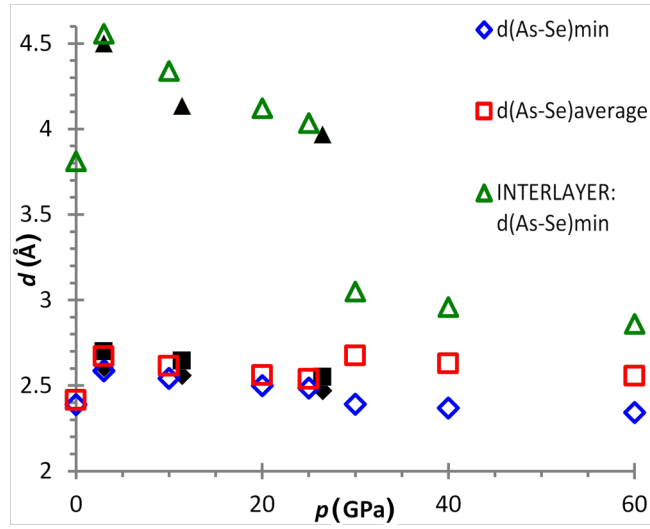

FIG. 5. The summary of the As–Se distances (intra- and interlayer) in the most relevant phases of As_2Se_3: phase **I** at 0 GPa, number of As–Se contacts, N(As–Se) = 3; phase **III** at 3–25 GPa, N(As–Se) = 6; phase **IV**, N(As–Se) = 7–8. The experimental data are shown as the black marks.

arises gradually, and may lead to the elongation of average As–Se bond length, as observed by Properzi *et al.* [50]. Therefore, while these are discontinuous phase transitions (first order) for the crystalline state, similar changes in coordination could happen continuously in the amorphous state. The transition from phase **III** to phase **IV** is related to a significant drop in interlayer As–Se distances, which now exceed the average "intralayer" As–Se distances by only 14% and are slowly approaching them during further compression. This is a clear sign of transition from the two-dimensional to quasi-three-dimensional system, which should strongly influence the electronic properties, similarly to the case of Sb_2Te_3 [29]. Indeed, the band-gap closure for *a*-As_2Se_3 takes place above 20 GPa, while metallic conductivity is achieved in this case close to 30 GPa [5]. Bearing in mind that the quasi-3D phase **IV** can be detected in our samples already above 20 GPa, this indicates that the pressure-influenced evolution of the amorphous and crystalline forms of As_2Se_3 should share common features.

ACKNOWLEDGMENTS

T.J. thanks the Polish Ministry of Science and Higher education for funding (Project "Mobility Plus" No. 1064/MOB/13/2014/0). T.J. and V.V.S. acknowledge Dr. Ross Hrubiak for the help in the XRD measurements, and Dr. Sergey Tkachev for Ne loading using the GSECARS gas loading system at APS. Use of the COMPRES-GSECARS gas loading system was supported by COMPRES under NSF Cooperative Agreement No. EAR-1606856 and by GSECARS through NSF Grant No. EAR-1634415 and DOE Grant No. DE-FG02-94ER14466. Portions of this work were performed at GeoSoilEnviroCARS (The University of Chicago, Sector 13), Advanced Photon Source (APS), Argonne National Laboratory. GeoSoilEnviroCARS is supported by the National Science Foundation Earth Sciences (Grant No. EAR-1634415) and Department of Energy–GeoSciences (Grant No. DE-FG02-94ER14466). Portions of this work were performed at HPCAT (Sector 16), Advanced Photon Source (APS), Argonne National Laboratory. HPCAT operations are supported by DOE-NNSA under Award No. DE-NA0001974 and DOE-BES under Award No. DE-FG02-99ER45775, with partial instrumentation funding by NSF. This research used resources of the Advanced Photon Source, a U.S. Department of Energy (DOE) Office of Science User Facility operated for the DOE Office of Science by Argonne National Laboratory under Contract No. DE-AC02-06CH11357.

[1] B. J. Eggleton, B. Luther-Davies, and K. Richardson, Nat. Photonics **5**, 141 (2011).
[2] J. T. Edmond, Br. J. Appl. Phys. **17**, 979 (1966).
[3] S. Hosokawa, Y. Wang, W.-C. Pilgrim, J.-F. Bérar, S. Mamedov, and P. Boolchand, J. Non-Cryst. Solids **352**, 1517 (2006).
[4] A. S. Ahmad, H. B. Lou, C. L. Lin, A. G. Li, K. Yang, K. Glazyrin, H. P. Liermann, H. Franz, K. Ståhl, S. Cui, B. Bureau, D. X. Zhang, X. D. Wang, Q. P. Cao, A. L. Greer, and J. Z. Jiang, Phys. Rev. B **94**, 195211 (2016).
[5] V. V. Struzhkin, A. F. Goncharov, R. Caracas, H. Mao, and R. J. Hemley, Phys. Rev. B **77**, 165133 (2008).
[6] A. C. Stergiou and P. J. Rentzeperis, Z Kristallogr. - New Cryst. Struct. **173**, 185 (1985).
[7] A. S. Kanishcheva, Y. N. Mikhailov, E. G. Zhokov, and T. G. Grevtseva, Neorg. Mater. **19**, 1744 (1983).
[8] A. A. Vaipolin, Kristallografiya **10**, 595 (1965).
[9] L. M. Lityagina, L. F. Kulikova, I. P. Zibrov, T. I. Dyuzheva, N. A. Nikolaev, and V. V. Brazhkin, J. Alloys Compd. **644**, 799 (2015).
[10] V. A. Kirkinskii and V. G. Yakushev, Dokl. Acad. Nauk SSSR **182**, 1083 (1967).
[11] W. Grochala, R. Hoffmann, J. Feng, and N. W. Ashcroft, Angew. Chem., Int. Ed. **46**, 3620 (2007).
[12] N. W. Ashcroft, Phys. Rev. Lett. **21**, 1748 (1968).
[13] N. W. Ashcroft, Phys. Rev. Lett. **92**, 187002 (2004).
[14] J. Feng, W. Grochala, T. Jaroń, R. Hoffmann, A. Bergara, and N. W. Ashcroft, Phys. Rev. Lett. **96**, 017006 (2006).
[15] M. I. Eremets, I. A. Trojan, S. A. Medvedev, J. S. Tse, and Y. Yao, Science **319**, 1506 (2008).
[16] T. Muramatsu, W. K. Wanene, M. Somayazulu, E. Vinitsky, D. Chandra, T. A. Strobel, V. V. Struzhkin, and R. J. Hemley, J. Phys. Chem. C **119**, 18007 (2015).
[17] A. P. Drozdov, M. I. Eremets, I. A. Troyan, V. Ksenofontov, and S. I. Shylin, Nature **525**, 73 (2015).
[18] I. Troyan, A. Gavriliuk, R. Ruffer, A. Chumakov, A. Mironovich, I. Lyubutin, D. Perekalin, A. P. Drozdov, and M. I. Eremets, Science **351**, 1303 (2016).
[19] M. Rivers, V. Prakapenka, A. Kubo, C. Pullins, C. Holl, and S. Jacobsen, High Pressure Res. **28**, 273 (2008).
[20] V. B. Prakapenka, A. Kubo, A. Kuznetsov, A. Laskin, O. Shkurikhin, P. Dera, M. L. Rivers, and S. R. Sutton, High Pressure Res. **28**, 225 (2008).
[21] C. Prescher and V. B. Prakapenka, High Pressure Res. **35**, 223 (2015).
[22] V. Petrícek, M. Dušek, and L. Palatinus, Z Kristallogr. **229**, 345 (2014).
[23] P. W. Stephens, J. Appl. Crystallogr. **32**, 281 (1999).
[24] See Supplemental Material at http://link.aps.org/supplemental/10.1103/PhysRevB.103.014103 for additional figures and datasets.
[25] R. J. Angel, M. Alvaro, and J. Gonzalez-Platas, Z. Kristallogr. **229**, 405 (2014).
[26] J. Gonzalez-Platas, M. Alvaro, F. Nestola, and R. Angel, J. Appl. Crystallogr. **49**, 1377 (2016).
[27] S. J. Clark, M. D. Segall, C. J. Pickard, P. J. Hasnip, M. I. J. Probert, K. Refson, and M. C. Payne, Z. Kristallogr. **220**, 567 (2005).
[28] P. A. Schultz and C. S. Snow, Modell. Simul. Mater. Sci. Eng. **24**, 035005 (2016).
[29] Y. Ma, G. Liu, P. Zhu, H. Wang, X. Wang, Q. Cui, J. Liu, and Y. Ma, J. Phys.: Condens. Matter **24**, 475403 (2012).
[30] S. Klotz, J. C. Chervin, P. Munsch, and G. Le Marchand, J. Phys. D: Appl. Phys. **42**, 075413 (2009).
[31] T. Scheler, O. Degtyareva, and E. Gregoryanz, J. Chem. Phys. **135**, 214501 (2011).

[32] S. M. Souza, C. M. Poffo, D. M. Trichês, J. C. de Lima, T. A. Grandi, A. Polian, and M. Gauthier, Phys. B (Amsterdam, Neth.) **407**, 3781 (2012).
[33] M. Einaga, A. Ohmura, A. Nakayama, F. Ishikawa, Y. Yamada, and S. Nakano, Phys. Rev. B **83**, 092102 (2011).
[34] L. Zhu, H. Wang, Y. Wang, J. Lv, Y. Ma, Q. Cui, Y. Ma, and G. Zou, Phys. Rev. Lett. **106**, 145501 (2011).
[35] K. Matsubayashi, T. Terai, J. S. Zhou, and Y. Uwatoko, Phys. Rev. B **90**, 125126 (2014).
[36] V. P. Cuenca-Gotor, J. A. Sans, J. Ibáñez, C. Popescu, O. Gomis, R. Vilaplana, F. J. Manjón, A. Leonardo, E. Sagasta, A. Suárez-Alcubilla, I. G. Gurtubay, M. Mollar, and A. Bergara, J. Phys. Chem. C **120**, 19340 (2016).
[37] Y. Zhang, Y. Ma, A. Geng, C. Zhu, G. Liu, Q. Tao, F. Li, Q. Wang, Y. Li, X. Wang, and P. Zhu, J. Alloys Compd. **685**, 551 (2016).
[38] J. Zhao, L. Yang, Z. Yu, Y. Wang, C. Li, K. Yang, Z. Liu, and Y. Wang, Inorg. Chem. **55**, 3907 (2016).
[39] T. J. Scheidemantel, J. F. Meng, and J. V. Badding, J. Phys. Chem. Solids **66**, 1744 (2005).
[40] C. Morin, S. Corallini, J. Carreaud, J. B. Vaney, G. Delaizir, J. C. Crivello, E. B. Lopes, A. Piarristeguy, J. Monnier, C. Candolfi, V. Nassif, G. J. Cuello, A. Pradel, A. P. Goncalves, B. Lenoir, and E. Alleno, Inorg. Chem. **54**, 9936 (2015).
[41] F. D. Murnaghan, Proc. Natl. Acad. Sci. USA **30**, 244 (1944).
[42] F. Birch, Phys. Rev. **71**, 809 (1947).
[43] J. Zhao, H. Liu, L. Ehm, Z. Chen, S. Sinogeikin, Y. Zhao, and G. Gu, Inorg. Chem. **50**, 11291 (2011).
[44] A. Jayaraman, B. Batlogg, R. G. Maines, and H. Bach, Phys. Rev. B **26**, 3347 (1982).
[45] B. Xu, Q. Wang, and Y. Tian, Sci. Rep. **3**, 3068 (2013).
[46] N. Soga, M. Kunugi, and R. Ota, J. Phys. Chem. Solids **34**, 2143 (1973).
[47] D. N. Nichols, D. S. Rimai, and R. J. Sladek, J. Non-Cryst. Solids **34**, 297 (1979).
[48] P. Haas, F. Tran, and P. Blaha, Phys. Rev. B **79**, 085104 (2009).
[49] L. G. Sillen, Ark. Kemi, Mineral. Geol. **12A**, 1 (1938).
[50] L. Properzi, M. Santoro, M. Minicucci, F. Iesari, M. Ciambezi, L. Nataf, Y. Le Godec, T. Irifune, F. Baudelet, and A. Di Cicco, Phys. Rev. B **93**, 214205 (2016).
[51] S. Hosokawa, Y. Sakaguchi, and K. Tamura, J. Non-Cryst. Solids **150**, 35 (1992).
[52] K. Tamura, S. Hosokawa, M. Inui, M. Yao, H. Endo, and H. Hoshino, J. Non-Cryst. Solids **150**, 351 (1992).
[53] M. Vaccari, G. Garbarino, S. N. Yannopoulos, K. S. Andrikopoulos, and S. Pascarelli, J. Chem. Phys. **131**, 224502 (2009).
[54] E. Soignard, S. A. Amin, Q. Mei, C. J. Benmore, and J. L. Yarger, Phys. Rev. B **77**, 144113 (2008).